RSC Advances

ROYAL SOCIETY OF CHEMISTRY

www.rsc.org/advances

Novel Green Phosphorescence from Pristine ZnO Quantum Dot: Tuning of Correlated Color Temperature

Abstract:

Creating novel functionality is always fascinating as well as advantageous from device point of view. We have tried with success to generate green phosphorescence, a novel phenomenon, in pristine zinc oxide quantum dots synthesized by an alkaline hydrolysis of a methanolic solution of zinc acetate dihydrate. The appearance of phosphorescence with radiative lifetime 4 – 22 μS is attributed to the singly charged oxygen vacancy ($V_{\dot{0}}$). Presence of $V_{\dot{0}}$s has been confirmed using electron paramagnetic resonance (EPR) and micro-Raman spectroscopy. In addition, an optimization of intensity and lifetime of phosphorescence has been made by tailoring the number of $V_{\dot{0}}$s and their variation has been satisfactorily explained on the basis of donor-acceptor pair recombination mechanism. Tailoring of the Commission Internationale de I'Eclairage (CIE) coordinates (x = 0.317, y = 0.544 in case of pristine ZnO quantum dots) of the synthesized quantum dots has been investigated in the presence of $V_{\dot{0}}$. Correlated Color Temperature of the quantum dots is evaluated and they are found to be suitable in cold light application.

Key words: Photoluminescence, time-resolved luminescence spectroscopy, chromaticity diagram, EPR, Raman spectroscopy

Sagnik Das[1], Chandan Kr. Ghosh[2,], Rajib Dey[3], Mrinal Pal[1,**]*

[1]Sensor and Actuator Division, CSIR- Central Glass and Ceramic Research Institute, Kolkata- 700032, West Bengal, India

**Corresponding authors e-mail ID: palm@cgcri.res.in

[2]School of Nanoscience and Technology, Jadavpur University, Kolkata- 700032, West Bengal, India

*Corresponding authors e-mail ID: chandu_ju@yahoo.co.in

[3]Department of Metallurgical and Material Engineering, Jadavpur University, West Bengal, India

Introduction:

Semiconductor nanomaterials are important building blocks in the grand architecture of nanotechnology because of their size-dependent novel electronic and optical properties originating from surface and quantum confinement effects. These semiconductors find wide applications in vacuum microelectronics, nanoscale electronic devices, light-emitting diodes, waveguides, sensors, laser technology, transparent high-power electronic materials, piezoelectric transducers, phosphors, solar cell to name a few.[1-12] Phosphors with high efficiency and lower degradation are important for the development of illumination technology and flat panel displays e.g. plasma display panels (PDP), field emission display (FED), vacuum fluorescent display (VFD).[13-17]Recently researchers are in search of biocompatible phosphors for in-vivo bio-imaging.[18]

Traditionally metal (cadmium, zinc, calcium, strontium, beryllium etc.) sulphides, selenides and tellurides are used as phosphors.[19-21] Cadmium is toxic. So also are sulphur, selenium and tellurium. Therefore they are not suitable for in-vivo bio-imaging. Again, sulphides, selenides and tellurides are not suitable for high vacuum applications like vacuum fluorescent display (VFD) because of their high vapour pressure.[22] They also emit contaminating gases. In contrast, metal oxide phosphors do not exhibit these drawbacks. However metal oxides alone do not show sufficient phosphorescence. This is achieved by doping with metal activators e.g. Cr^{3+}, Mn^{2+}, Ce^{3+}, Eu^{2+}, Eu^{3+}, Tb^{3+}, Tm^{3+}etc. [23]

Zinc oxide (ZnO) is a direct wide band gap (3.37eV), low refractive index (1.90-2.00), non-toxic semiconductor with high exciton binding energy (60meV).[24-26] The PL spectra of ZnO usually consists of two typical emission bands: one in the ultra-violet (UV) region attributed to the band edge transition or the exciton combination and the other in the visible region attributed to different crystalline defects e.g. oxygen vacancies, zinc vacancies, zinc interstitial etc. ZnO shows phosphorescence in the visible range when doped with costly rare lanthanides (e.g. Eu^{3+}) or when are made composites with other sulphides, selenides or tellurides (CdS, ZnS etc.).[23,19] Thin films of zinc doped zinc oxide formed by sputtering show phosphorescence with lifetime of the order of 1-10 µS.[17] Only, very recently, there has been a paper reporting the presence of phosphorescence in pristine ZnO nanorods. However the lifetime is not significantly high at room temperature (on an average ~2.4 µS).[27]To the best of our knowledge, until now there is no report on the phosphorescence of pristine ZnO quantum dots (QDs) having an average life time of ~ 26 - 18 µS.

In this article we report for the first time the high lifetime of green phosphorescence of the order of 10-100 µS in pristine ZnO QDs prepared by a facile, green technique. Secondly we report the correlation of the emission properties of the ZnO QDs with the variation of oxygen vacancies induced by low temperature annealing. Lastly, we report on the theoretical interpretation of the systematic variation of the radiative and non-radiative lifetime as well as the intensity of the green phosphorescence exhibited by ZnO QDs. Thus these ZnO QDs would possibly find use in some lighting applications, especially in display tubes and VFDs where lifetimes ~ 10 µS are expected.

Experimental

Materials & Method

ZnO QDs were prepared by the hydrolysis of zinc acetate dihydrate ($Zn(CH_3COO)_2.2H_2O$, E-Merck, India) in an alkaline methanol solution as reported by D. Sun *et al* [28] and the larger sized ZnO nanoparticles were prepared by hydrolysis of zinc acetate dihydrate in an alkaline aqueous solution. Briefly, 0.896 g (16 mmol) potassium hydroxide (KOH, E-Merck, India) was dissolved in 150 ml of methanol (E-Merck, India). This solution was refluxed at 55°C for half an hour for proper homogenization. Separately, 1.756 g (8 mmol) zinc acetate dihydrate was dissolved in 50 ml methanol and stirred for 15 minutes at room temperature to obtain a homogeneous solution. This solution was directly added to the KOH solution stirring at 55°C and this mixed solution was refluxed for another 2 hours at the same temperature. Subsequently, the clear sol, obtained after 2 hours, was concentrated 10 times at 30°C via rotary evaporation under vacuum. Hexane (E-Merck, India) and isopropanol (E-Merck, India) was added to this concentrated sol in a volume ratio of ZnO sol: hexane: isopropanol = 1: 5: 1 to precipitate out ZnO QDs. The white precipitate thus obtained was collected after centrifugation at 6000 rpm (REMI, R - 24). The collected powder was dried at 110°C for 2 hours (named as ZQD). Subsequently ZQD samples were heated at 150°C in a charcoal boat under the flow of nitrogen for 1 hour and 2 hours respectively and the samples thus prepared are designated as ZCF1 and ZCF2 respectively. All the reagents were of analytical grade and were used without further purification.

In a typical synthesis of larger sized ZnO nanoparticles, calculated amount of zinc acetate dihydrate was dissolved in water taken in a beaker. In another beaker calculated amount of potassium hydroxide was dissolved in water. Hereafter these two solutions were mixed and refluxed at 100°C for 2 hours. The precipitate thus obtained was collected by centrifugation at 6000 rpm and dried overnight in an oven at 60°C (named as ZNC).

Characterization

X-ray diffraction (XRD) patterns of all the samples were taken by Ultima III diffractometer (Cu K_α radiation, λ = 1.5404Å, Rigaku, Japan) to identify phases of the synthesized samples. Morphology and size distribution of the samples were investigated by transmission electron microscope (TEM, JEOL 2100) operating at 200 kV. For TEM analysis, samples were dispersed in methanol by ultrasonication (250W) and were drop cast onto a carbon coated copper grid. The TEM images and the First Fourier Transformation (FFT) carried out on the TEM images, are used to identify the morphology and the phase purity of the samples. Room temperature micro-Raman spectra of the synthesized samples were recorded using alpha 300, WITEC, Germany having laser source at 532 nm. Photoluminescence spectra were taken at room temperature to investigate the defect induced emission and their systematic variation in intensity as a function of annealing time, by using a spectrofluorometer (Shimadzu RF5301), having a Xe lamp source with an excitation wavelength of 300 nm. The Commission Internationale de I'Eclairage (CIE) coordinates were calculated for the emission spectrum which is the superimposition of different emission spectra weighted to their concentrations. Lifetime of the photogenerated electrons within the naoparticles was investigated by using time resolved PL (Edinburgh FLSP-980) spectroscopy. Electron paramagnetic resonance (EPR) spectra were recorded at room temperature using (JEOL – JES FA 200) spectrophotometer operating in the X-band frequency (9.41 GHz) with a field modulation frequency of 100 kHz.

Results and discussion

Structural analysis of the sample by x-ray diffraction, high resolution transmission electron microscopy and micro-Raman spectroscopy

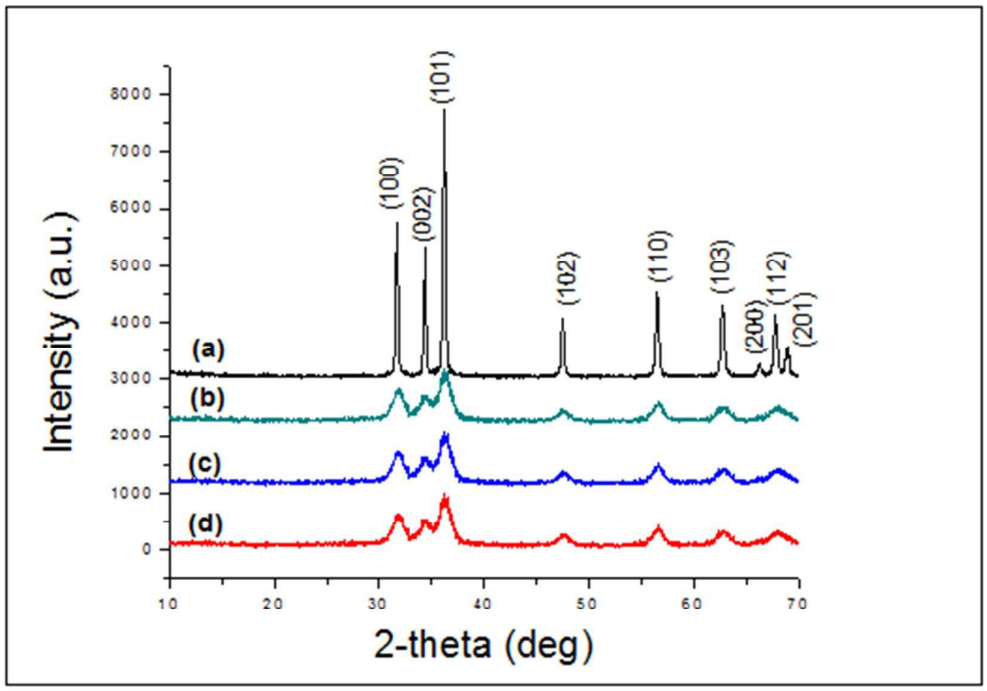

Figure 1: X-ray diffraction pattern of (a) ZNC, (b) ZQD, (c) ZCF1 and (d) ZCF2.

Figure 1 shows the XRD patterns of ZQD, ZCF1, ZCF2 and ZNC. Nine diffraction peaks can readily be indexed by the Bragg's reflection from (100), (002), (101), (102), (110), (103), (200), (112), (201) planes of wurtzite ZnO (JCPDS Card NO. 36-1451). Absence of any other peak in the pattern indicates the purity of the crystalline ZnO nanoparticles.

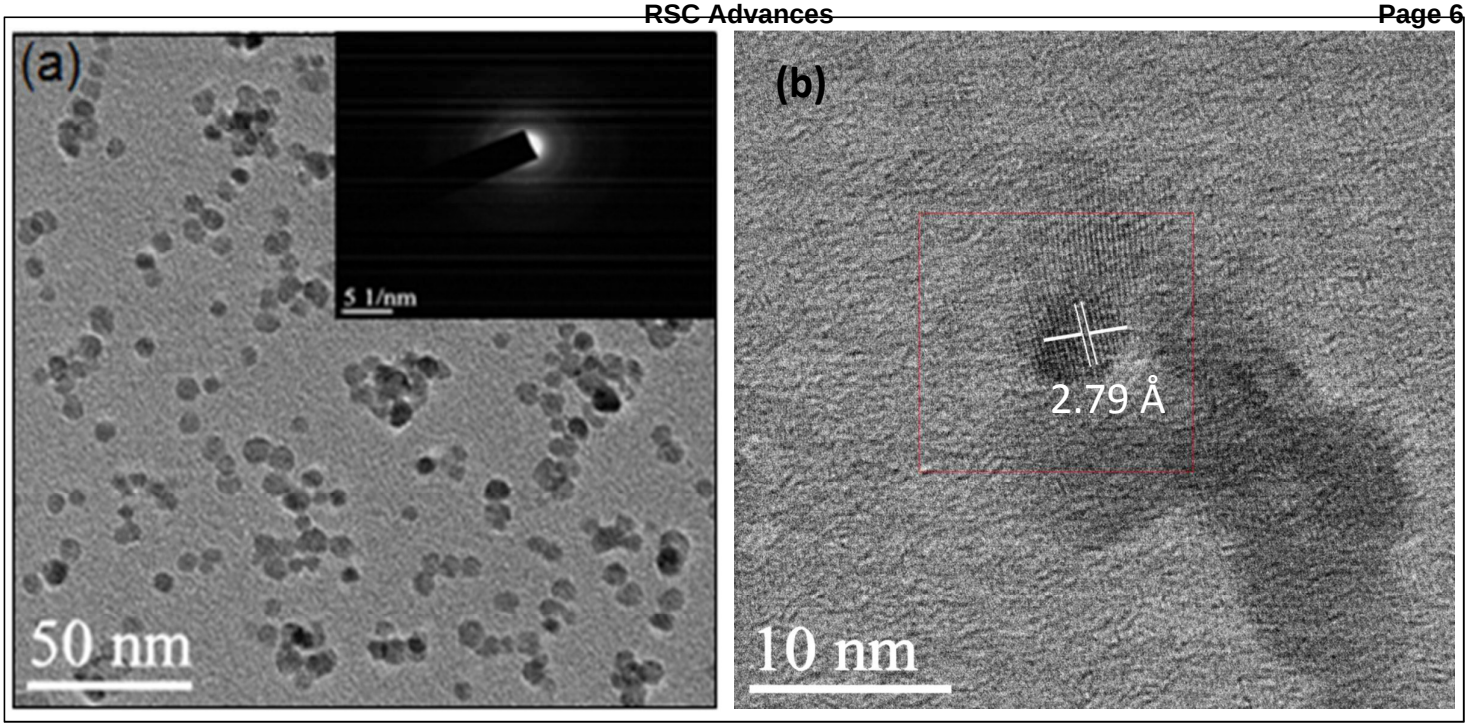

Figure 2: (a) TEM image, (b) HRTEM lattice image of the ZQD samples.

Figure 2(a) shows typical TEM image of ZQD and it is clearly revealed from the image that the ZQD sample consists of uniform distribution spherical quantum dots. It is evident from the figure that the synthesized samples possess uniform darkness throughout the sample indicating solid nature of the nanoparticles. The histogram representing the particle size distribution of ZQDs has been constructed from the TEM image **Figure 2(a)**. The Gaussian fit to this histogram (ESI, figure S1) supported the uniform distribution of the QDs. The average size of the QDs obtained from this distribution is 5.38 ±0.87 nm. Interplanar spacing d= 0.279 nm, represented in **Figure 2(b)**, matches well with the standard $d_{(100)}$ = 0.281 nm of ZnO (JCPDS Card NO. 36-1451). Lattice fringes in the image indicate high crystallinity of the nanocrystalline ZnO. TEM images and the size distribution corresponding to ZCF1, ZCF2 and ZNC are presented in ESI (Figures S1 – S2).

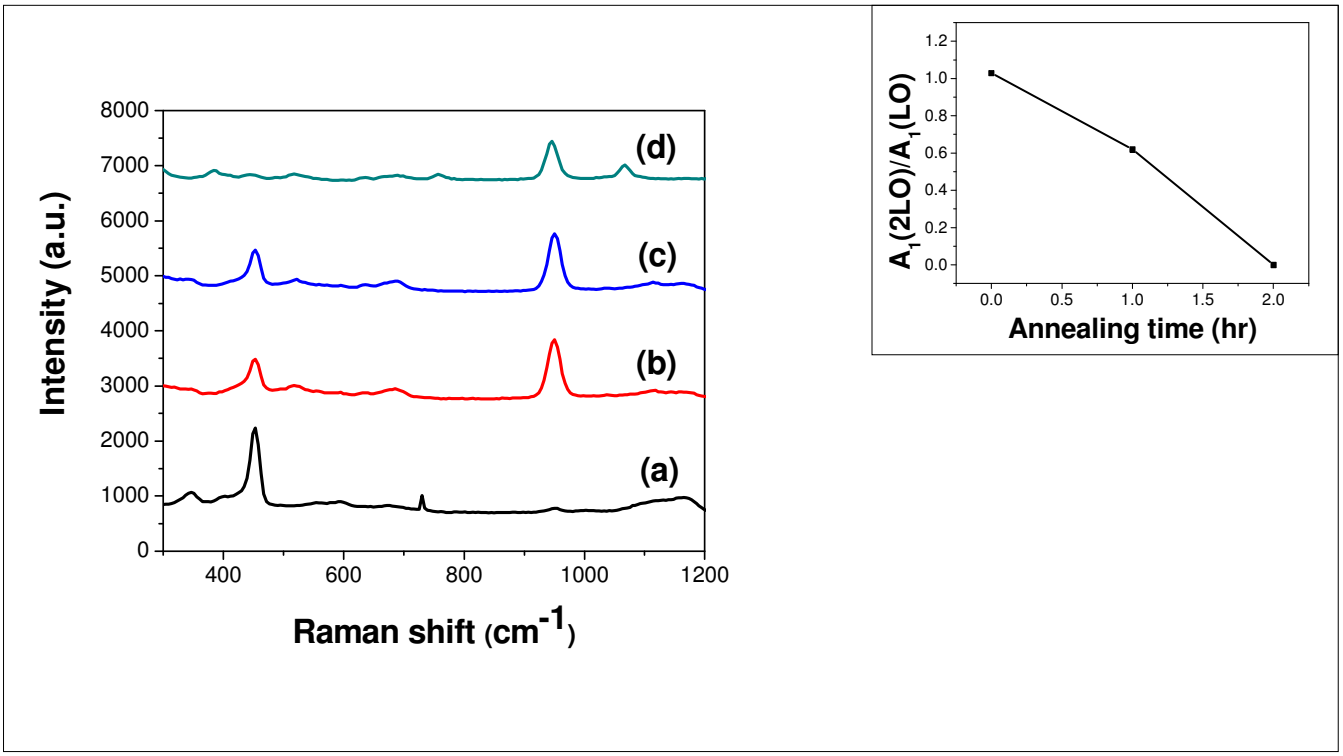

Figure 3: Micro-Raman spectra of (a) ZNC, (b) ZQD, (c) ZCF1 and (d) ZCF2. Inset represents the intensity ratios of $A_1(2LO)/A_1(LO)$ as a function of annealing time.

Figure 3 depicts the micro-Raman spectra of ZNC, ZQD, ZCF1 and ZCF2 and their magnified version are presented in ESI (Figure S3) for easy identification of the Raman peaks and the table containing the corresponding data are also presented in ESI (Table S4). It is observed from figure that the Raman spectrum of ZNC consists of four highly intense major peaks and few peaks with low intensity. The peak, obtained at 451 cm^{-1}, is associated nonpolar phonon vibrational mode of oxygen sublattice with E_2 symmetry and is the fingerprint of wurtzite crystal structure of ZnO.[29, 30] The peak, identified at 345 cm^{-1}, is attributed to the $E_2(high) - E_2(low)$ mode of vibration.[29] Peaks, measured at 593 and 1164 cm^{-1}, originate from first and second order vibration of intrinsic lattice defects e.g. V_O with A_1 symmetry ($A_1(LO)$, $A_1(2LO)$).[31, 32] In addition to the conventional phonon modes, less intense peak, obtained at 558 cm^{-1}, may be ascribed to the surface phonon.[29] The peaks at 685 and 400 cm^{-1} are attributed to the TA + LO phonon mode [29] and first order $A_1(TO)$ mode vibration [33,34] respectively. The peak at 729 cm^{-1} corresponds to second order $E_{2L} - B_{1H}$ phonon mode. In the case of ZQD, six peaks have been identified. The peaks, observed at 345, 451 and 685 cm^{-1} may be assigned to ($E_2(high) - E_2(low)$ and oxygen sublattice $A_1(LO)$ and TA + LO phonon mode respectively. It is interesting to note that the energy corresponding to $E_2(high) - E_2(low)$ or oxygen sublattice or TA + LO remains unchanged in ZQDs compare to ZNC. The peak, measured at 518 cm^{-1}in ZQD, may be

ascribed to surface phonon mode. Less intense peaks, found at 583 and 1116 cm^{-1}, are attributed to the A_1(LO) and A_1(2LO) mode of vibration. The Raman spectrum of ZCF1 is found to be identical to that ZQD except differences in intensities of a few peaks. Four peaks at 384, 444, 518, 685 cm^{-1} have been observed for ZCF2 sample. In this context, it may be stated that the energy corresponding to E_2(high) – E_2(low), measured at 384 cm^{-1} vibration increases in ZCF2 compared to others, whereas energy of oxygen sublattice mode, measured at 444 cm^{-1}decreases. Interestingly Raman shifts corresponding to surface phonon (at 518 cm^{-1}) and TA + LO mode (at 685 cm^{-1}) remain unchanged compared to ZQD. A_1(2LO) vibrational peak is found to be absent in ZCF2. Intensity ratios of A_1(2LO) and A_1(LO) modes of vibrations that represent the charge carrier – phonon coupling strength, are calculated for ZQD, ZCF1 and ZCF2 and are shown in the inset of **Figure 3**.[29] It is clear from the figure that the ratio exhibits the maximum value for ZQD followed by gradual decrease from ZCF1 to ZCF2. This result indicates that charge carrier – LO phonon interaction successively decreases with increasing annealing time. Therefore, it may be concluded that the phonon vibration corresponding to the oxygen deficient sample generates the local electric field that strongly polarizes the surrounding electrons and holes. During annealing, oxygen deficiency decreases within the samples, hence polarization of electrons due to lattice vibration i.e. charge carrier – phonon interaction decreases. This phenomenon has an important bearing on the lifetime of photo-generated electrons as will be explained latter.

Investigation on the optical properties of the samples by photoluminescence spectroscopy and time resolved photoluminescence spectroscopy

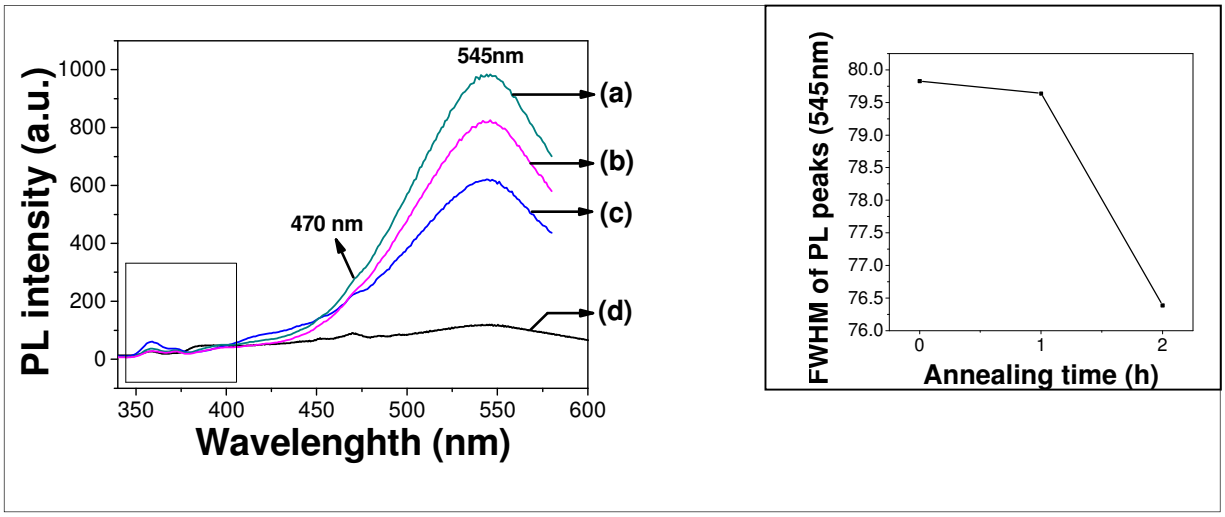

Figure 4: Plot of photoluminescence intensity versus wavelength for: (a) ZQD, (b) ZCF1, (c) ZCF2, (d) ZNC. Inset shows the plot of FWHM of PL peaks vs. annealing time.

In order to investigate the impurity states formed within band gap and associated optical emissions, we have measured photoluminescence (PL) property of the synthesized samples (ZQD, ZFC1, ZFC2 and ZNC) at room temperature under identical condition after excitation at 300 nm. Spectra of the samples, presented in **Figure 4**, possess typical luminescence property having emission in the UV range and broad deep-level-emission (DLE) in the visible range. The inset contains the plot of FWHM of green emissions of ZnO QDs as a function of annealing time. The UV region of the PL spectra has been enlarged and is presented in ESI (Figure S5) for easy identification of the emission peaks. In general, UV emission originates from the direct recombination of photogenerated charge carriers, while the visible emission spectra are attributed to the electronic transition involving various defects such as neutral vacancies, charged vacancies, interstitial sites etc.[26, 35] PL spectrum of ZQD shows two UV emission peaks at 357 and 371 nm, blue emission peak at 470 nm and a violet emission peak at 396 nm. These peaks may be attributed to the band to band transition, excitonic transition, [36] interstitial Zn (Zn_i) to zinc vacancy (V_{Zn}) and transition from the conduction band to V_{Zn} respectively. [37]From the luminescence spectrum the energy computed for band to band transition is 3.47 eV, whereas energy involved in electronic transition between conduction band and V_{Zn} is 3.13 eV. Therefore, we may conclude that V_{Zn} that acts as a shallow electron acceptor state with the energy level 0.34 eV above the valence band. The broad intense peak for green emission at 545 nm corresponding to ZQD may be ascribed to the transition of electron from singly charged oxygen vacancy ($V_O^{\cdot}$) to zinc vacancy (V_{Zn}) sites. EPR spectra of ZQD, ZFC1 and ZCF2 (shown in ESI, Figure S6) also confirm the presence of $V_O^{\cdot}$ in the synthesized samples. The important point to mention here is that our synthesized ZQDs don't possess any violet emission as obtained by other researchers. [38] The PL spectrum of ZCF1 is found to be similar to that of ZQD except the difference in their intensities corresponding to the green emission. In addition to the UV and green emissions, the emission peak at 430 nm observed for ZCF2 may be attributed to electronic transition between the Zn_i and the valence band. Presence of such Zn_i may be attributed to the displacement of $Zn^{2+}$from its regular position due to the diffusion of oxygen atoms from the surrounding atmosphere during annealing. From the calculation by Zhang *et al.*, we may conclude that Zn_i produces the shallow deep donor level at 2.88 eV above the valence band.[39] Significantly, we observed no change in peak position corresponding either to the UV or the visible emissions of ZQD, ZCF1 and ZCF2 and this observation signifies that the particle size remains unchanged during the annealing of the samples. This result is further corroborated by the unchanged particle size computed from the XRD and TEM. In order to differentiate the PL property of quantum dots with that of larger sized ZnO particles (ZNC), we have measured the PL spectrum of ZNC that consists of two UV emission peaks at 357 and 384 nm, blue emission at 470 nm and green emission at 545 nm. Though, energies corresponding to band-to-band transition, blue emission and green emission don't change for ZNC, but energy corresponding excitonic emission decreases due to change in the exciton binding energy. It has been observed that intensity of the green emission successively decreases from ZQD to ZCF1 to ZCF2. Most importantly, the intensity of green emission gets significantly reduced in ZNC samples. In general, luminescence intensity is found to be proportional to the number of luminescent centres and inversely proportional to the lifetime of the excited electron.[40] In the present case, number of luminescent centres corresponding to the green emission i.e. $V_O^{\cdot}$ gets reduced during heating the ZnO QD samples in N_2 atmosphere. [38] This could be explained qualitatively as follows: the formation of charged oxygen vacancy can be represented by the following defect equations using the Kröger – Vink notation:

$$O_O = {}^{1}/_{2}O_2 + V_0$$

$$V_0 = V_o^{\cdot} + e'$$

$$O_O = 1/2\ O_2 + V_o^{\cdot} + e' \qquad (1)$$

Assuming that $[V_o^{\cdot}] = [e^{'}]$ the equilibrium constant (K) of equation (1) can be written as:

$$K = p_{o2}^{1/2} \cdot [V_o^{\cdot}]^2 \qquad (2)$$

Thus when $V_o^{\cdot}$ is very high at the beginning (as evident from PL and EPR signal of QD compared to ZNC) equilibrium partial pressure p_{o2} is extremely low, lower than the oxygen partial pressure of controlled nitrogen atmosphere. Thus when the QDs are heat treated at 150°C for 1 hour and 2 hours in nitrogen atmosphere in a charcoal boat, oxygen from the surrounding atmosphere of high oxygen partial pressure will be consumed by the QDs in order to achieve the lower equilibrium partial pressure of oxygen. Thereby oxygen vacancies are decimated during heating. In order to get more insight into the intense green emission process, we have fitted the emission spectrum by Gaussian curve (FigureS7 (A), ESI) and have obtained the full width at half maxima (FWHM) of each spectrum that gets reduced from ZQD to ZCF1 to ZCF2 as presented in the inset of **Figure 4**. The FWHM of the emission spectra significantly depends on the nonradiative transition which in consequence is determined by the charge carrier - LO phonon interaction.[41, 42] In this context, it may be stated that Huang – Rhys factor (S) has been defined to attribute the nonradiative transition and mathematically is found to be proportional to the square of FWHM corresponding to the photoluminescence emission spectra (detailed discussion is presented in S7(B), ESI). [41] Therefore the reduction in FWHM indicates the reduction of the charge carrier - LO phonon interaction and nonradiative transition rate with annealing. Raman analysis also predicts the similar type of reduction in the charge carrier - LO phonon interaction.

The time-resolved PL (τ-PL) spectra (Figure S - 8, ESI), taken at room temperature, were employed in an effort to determine the lifetime more deeply and to investigate details of the recombination mechanism (radiative or non-radiative) of intense green emission corresponding to ZQD, ZCF1 and ZCF2 after exciting them at 300 nm using microsecond Xenon flash lamp. Careful analysis of the emission spectra reveals that all the spectra could be satisfactorily fitted (least-squares fitting method) by triple-exponential decay function: $B_1\exp(-t/\tau_1) + B_2\exp(-t/\tau_2) + B_3\exp(-t/\tau_3)$, where τ_i and B_i (i = 1, 2, 3) represent the time-constant and normalized amplitude of contribution respectively. [43] After fitting, it has been observed that the green emission spectrum of the ZnO quantum dots consist of three life-times having different amplitude (presented in details in ESI, Table S - 9). S - 10 (in ESI) contains the standard deviation of the fitted data of S-9.

The presence of three different lifetimes signifies the presence of three different decay or capture process in this green emission process. Amplitude of τ_3 is found to be very insignificant compared to τ_1 and τ_2 for all the samples; hence its contribution is neglected for the present analysis. The first decay contribution (B_1) is noticed to be dominating over the second one (B_2) for all the samples. Further, it is noticed that τ_1 which may be attributed to the non-radiative recombination of shallow

trapped electrons and shallow trapped holes increases with annealing time whereas the intensity of the emission decreases.[44] This is also elaborated in S – 11 of ESI. Completely opposite phenomenon has been observed both in terms of the lifetime $\tau_2$and the associated intensity of emission originating from the radiative recombination within quantum dots.[45] Importantly, the decay process corresponding to this emission is found to be of the order of µS, whereas other researchers noticed time-constant of the order of nanosecond or picosecond for band to band UV emission.[45, 37, 41] In this context, it may be stated that green emission lifetime ~ µS has been reported in Eu doped ZnO and ZnO nanorods by Armelao *et al.* [46] and He *et al*. [27] respectively. Such high value of the decay time-constant was investigated by several researchers in terms of deeper trap and less shallow trap states. [47] In recent time, Studenikin *et al.* explained the µS lifetime on the basis of electron – hole recombination in a donor-acceptor complex. [48] In this context, it has to be mentioned that energy-state [49] and the electron-phonon coupling model [41] were also developed to describe such high value of the decay time. In general, decay rate of the photoluminescence process is determined by the photo-luminescence time-constant (τ_{PL}) which in turn is described by the radiative (τ_R) and non-radiative (τ_{NR}) time-constants as given by${\tau_{PL}}^{-1} = {\tau_R}^{-1} + {\tau_{NR}}^{-1}$.The longer lifetime that we obtained after fitting may be attributed to the radiative donor-acceptor pair (DAP) recombination in which $V_{\dot{0}}$ acts as shallow donor level, whereas $V_{Zn}^{'}$ forms the shallow acceptor level. It is clear from **Figure 5** that radiative lifetime decreases whereas its amplitude increases with the annealing time. Within DAP recombination mechanism, the radiative recombination rate, $W_R\left(=\frac{1}{\tau_R}\right)$, may be written in terms of the optical matrix elements between the state (ψ_i) of the crystal that formed by an electron bound to a specific donor and a hole bound to a acceptor and the state (ψ_f) of the crystal in empty condition [50] and is described by equation (3)

$$W_R \propto \left|\int \psi_f P \psi_i dv\right|^2 \qquad (3)$$

where P represents the momentum operator. In the case when they are not tightly bound to the crystal, the radiative recombination rate can be expressed as, [51,52]

$$W_R(r) = W_R e^{-2r/a_B} \qquad (4)$$

Where r and a_B represent the delocalization of the electron-hole pair and Bohr radius respectively. From intensed green emission band, we may conclude that our synthesized ZnO quantum dots contain high concentration of $V_{\dot{o}}$ and forms impurity band. During annealing the sample, $V_{\dot{o}}$ gets reduced asexplained earlier i.e. width of the impurity band decreases that results in decrease in delocalization of the electron. Hence $W_R(r)$ increases with annealing and consequently the radiative lifetime decreases.

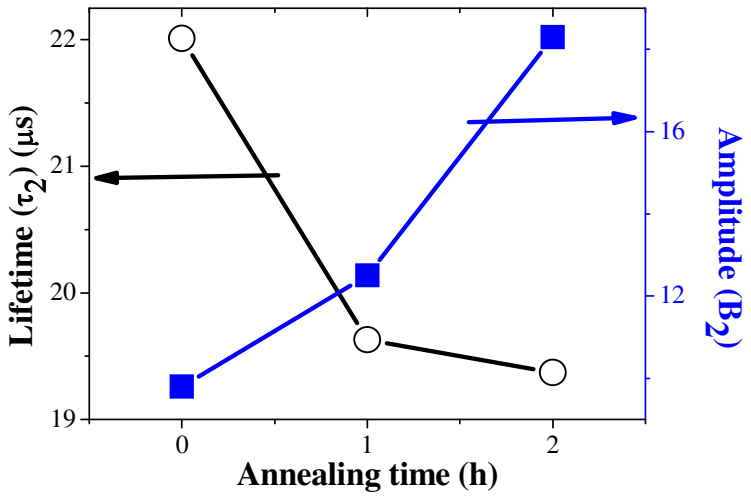

Figure 5: Variation of radiative life time and PL intensity of ZnO QDs as a function of annealing time.

The other lifetime (τ_1) may be ascribed to the non-radiative part of the green emission. In contrast to radiative lifetime, it has been observed that non-radiative lifetime increases whereas a sharp reduction in its amplitude has been observed with increasing annealing time (**Figure 6**). From the Raman and photoluminescence intensity pattern, it was concluded that the ZnO QDs possess strong charge carrier – LO phonon interaction that successively decreases with annealing the samples as described earlier. Therefore, the nonradiative DAP recombination that involves high energy ~ 2.29 eV may be attributed to the interaction of charge carriers within the impurity band – LO phonon having frequency ω_{LO}. In order to understand the variation of nonradiative lifetime, we consider Huang – Rhys factor (S) that is generally used to express the charge carrier – LO phonon interaction and is given by the following equation, [53]

$$S = \sum_q \frac{|V_q^2|}{(\hbar\omega_{LO})^2} |\rho_q|^2 \qquad (5)$$

Where, V_q and ρ_q represent the strength of the carrier – LO phonon interaction and Fourier transform of the charge density respectively. '$\hbar$'is the reduced Planck's constant. For DAP recombination process 'S' is simplified to the following relation,

$$S = \left(\frac{1}{\epsilon_\infty} - \frac{1}{\varepsilon_0}\right)\frac{e^2}{a_h}\frac{1}{\hbar\omega_{LO}}\left\{\frac{5}{16}(1+\sigma) + \frac{a_h}{R}[(\Delta_e + \Delta_h)(1-\sigma^2)^{-3} - 1]\right\} \qquad (6)$$

Where, $\epsilon_\infty(\varepsilon_0)$ and a_h are the high (static) frequency dielectric constant and the orbital radius for hole respectively. $\sigma$and R represent the ratio of orbital radii of hole to electron (= a_h/a_e) and the distance between them respectively. The parameters, Δ_e and Δ_h, are given by the following equations:

$$\Delta_e = \left[1 - 3\sigma^2 + (1 - \sigma^2)\frac{R}{a_e}\right]\exp\left(-\frac{2R}{a_e}\right) \quad (7)$$

and,

$$\Delta_h = \sigma^4\left[3 - \sigma^2 + (1 - \sigma^2)\frac{R}{a_h}\right]\exp(-\frac{2R}{a_h}) \quad (8)$$

It has been predicted earlier that V_0concentration gets reduced during annealing the as synthesized quantum dots in N_2 atmosphere. Hence we assume that the average distance between donor and acceptor increases from R to R + ΔR. As R increased to R + ΔR, assuming ΔR<<R the first order change in the value ofΔ_e and $\Delta_h$to $\Delta_e'$and Δ_h' respectively can be given by,

$$\Delta_e' = \Delta_e - [2(1 - \sigma^2)\frac{R}{a_e} + 1 - 5\sigma^2]\frac{\Delta R}{a_e}\exp\left(-\frac{2R}{a_e}\right) \quad (9)$$

and,

$$\Delta_h' = \Delta_h - \sigma^4[2(1 - \sigma^2)\frac{R}{a_h} + 5 - \sigma^2]\frac{\Delta R}{a_h}\exp\left(-\frac{2R}{a_h}\right) \quad (10)$$

Thus from above equations it is clear that the value of $\Delta_e'$and Δ_h' gets reduced due to enhancement of the average distance (ΔR > 0) between donor and acceptor. Hence, reduction in the 'S' parameter i.e. electron – LO phonon interaction results in the enhancement of the corresponding non-radiative lifetime.

.

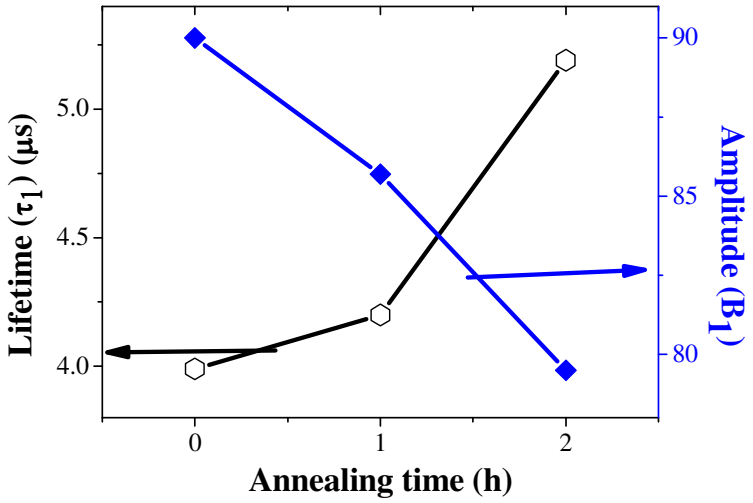

Figure 6: Variation of non-radiative life time and intensity of PL as function of annealing time of ZnO QDs.

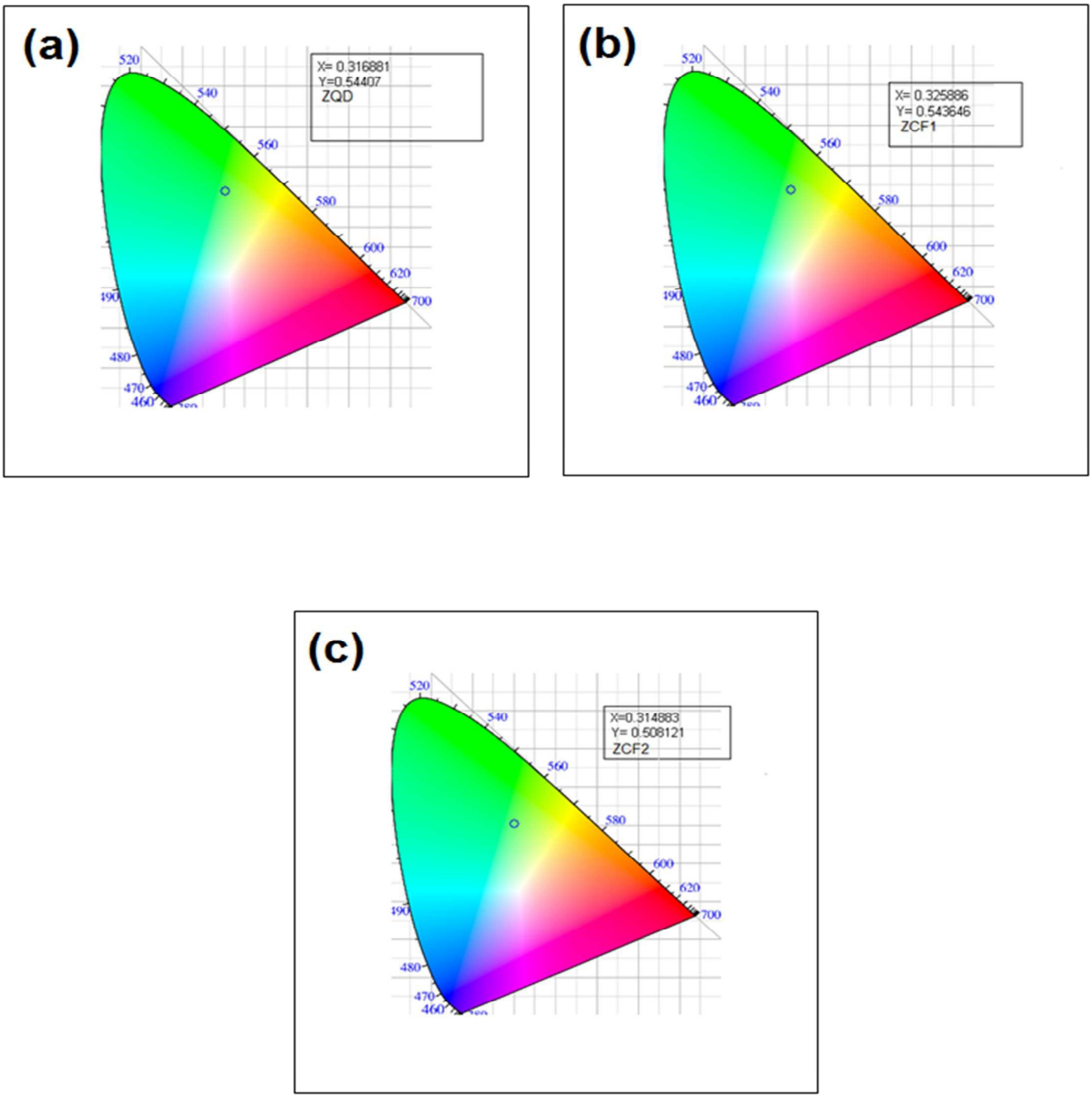

Figure 7: Chromaticity plot of(a) ZQD, (b) ZCF1, (c)ZCF2.

To evaluate the pixels behaviour of the synthesized quantum dots, the emission colour coordinates (x, y), known as CIE 1931 chromaticity coordinates, were calculated at an excitation wavelength300 nm. This procedure offers more precise colour measurement because the parameters are evaluated on the basis of spectral power distribution (SPD) of the light, emitted from the coloured object. The emitted colour which is the superposition of three primary colours (blue, green and red) is represented on the chromaticity diagram (**Figure 7(a) – (c)**) by a triangular gamut that is generated by joining three coordinates corresponding to three primary emissions at its corners. For instance, it is clear from chromaticity diagram that ZQD, ZCF1 and ZCF2 exhibit chromaticity coordinates (0.317, 0.544), (0.326, 0.544) and (0.315, 0.508) respectively. Thus the emission can be easily tuned by annealing. The correlated colour temperature (CCT), is calculated from the well-known McCamy's relation,[54], given by, CCT = $449n^3 + 3525n^2 + 6823.3n + 5520.3$, where n = (x - 0.3320) / (0.1858 - y) and (x, y) represents the chromaticity co-ordinates. Using the chromaticity co-ordinates for ZQD, ZCF1, ZCF2 in the above equation, the correlated colour temperatures have been computed as 5812.4K, 5635.9K and 5890.4K respectively. Therefore the synthesized quantum dots may be suitable for cool light application. Quantum yields, calculated from the following equation, are found to be 0.15, 0.18 and 0.21 for ZQD, ZCF1 and ZCF2 respectively.[55, 56]

$$QY = \frac{{}^{1}/_{\tau_2}}{{}^{1}/_{\tau_2} + {}^{1}/_{\tau_1}} \qquad (11)$$

Interestingly, quantum yield of ZnO quantum dots, dispersed in ethanol (3 - 5%), [57] or excitonic emission corresponding to bulk ZnO (0.016),[58] was measured to be very low compare to our synthesized samples.

Conclusion

Pristine ZnO QD was prepared by a facile, green synthesis technique. This is for the first time we are reporting the phosphorescence having lifetime between10μs -100 μs in pristine ZnO QDs. This unique green phosphorescence of the as prepared and heat treated quantum dots arises due to the presence of singly charged oxygen vacancies ($V_{\dot{0}}$). It was further observed that the PL intensity decreases gradually with increasing annealing time at 150°C in a charcoal boat in nitrogen atmosphere. This leads to the understanding that the as prepared quantum dots was so rich in V_0that even the low oxygen partial pressure in the atmosphere was sufficient for the annihilation of such defects. The systematic variation of the radiative and non-radiative life time, as well as the intensity of the green phosphorescence of pristine ZnO QDs as function of annealing time has been satisfactorily explained by using theoretical models. It was understood from these analyses that a provident optimisation of the particle size somewhere in between quantum dot and bulk ZnO would lead to maximum radiative lifetime resulting in the fullest exploitation of this material as a phosphor. Also the colour temperatures of the QDs were calculated from their respective CIE plots. The ZnO QDs due to their green emission with a lifetime of 10-100μs and correlated colour temperature in the

range of 5600-5900 K may find applications in illumination technologies, especially VFDs, display tubes and cool lighting.

Acknowledgement

We gratefully acknowledge the Principal, Belur Vidyamandir for providing support on PL and τ-PL measurements. The UPE-II programme, Jadavpur University and Department of Chemistry, Jadavpur University are gratefully acknowledged for experimental help on TEM, Raman Spectroscopy and EPR. We gratefully acknowledge G. C. Das, Professor, Department of Metallurgical and Material Engineering, Jadavpur University for helpful discussion throughout the course of the work.

References

1. Debabrata Sarkar, Chandan. K. Ghosh and Kalyan K. Chattopadhyay, *Cryst. Eng. Comm.*, 2012, 14, 2683.

2. X Duan, Y Huang, Y Cui, J Wang,CM Lieber, *Nature*, 2001, 409, 66.

3. Semiconductor light emitting diode: YasuyukiSakaguchi (University of Tokyo), Sigemasa Nakamura (Nagoya University), Yasuo Hosokawa (Chichibu Research laboratory), Yutaka Saito, *Japan,US 5656829A*, 1997.

4. J. Mørkand A. Mecozzi, *Journal of the Optical Society of America B*, 1996, 13,1803.

5. Simon M. Sze (Editor), *Semiconductor Sensors*, JohnWiley & amp, New York, USA1994.

6. Infrared and Visible Semiconductor Lasers, a) Govind P. Agrawal, b) Niloy K. Dutta, *Semiconductor Lasers*, Springer-Verlag, USA 1993, 547.

7. Kenji Nomura, HiromichiOhta, Kazushige Ueda, Toshio Kamiya, Masahiro Hirano, Hideo Hosono; *Science*, 2003, *300,* 1269.

8. Shenai, K, Scott, R.S. Baliga, B.Jayant, *Electron Devices*, *IEEE Transactions*, 1989, 36,1811.

9. Marc-Alexandre Dubois, Paul Muralt, *Appl. Phys. Lett*., 1999, 74, 3032.

10. Xiao Zhang , Wei Liu , George Z. Wei , Debasis Banerjee , Zhichao Hu , Jing Li, *J. Am. Chem. Soc*., 2014, 136 (40), 14230.

11. Q. Dai, J. Chen, L. Lu, J. Tang, W. Wang, *Nano Letters*, 2012, 12, 4187.

12. O'Regan B, Grätzel M, *Nature,* 1991, 353, 737.

13. Ming Qiao, Bo Zhang , Zhiqiang Xiao , Jian Fang , Zhaoji Li, Power Semiconductor Devices and IC's, ISPSD '08. 20th International Symposium, 18-22 May 2008, 52.

14. A. Morell and N. El Khiati, *J. Electrochem. Soc*. ,1993,140, 2019.

15. N. Hirosaki, R.-J.Xie, K. Inoue, T. Sekiguchi, B. Dierre, K. Tamura, *Applied Physics Letters*, 2007, 91, 061101.

16. MarkkuLeskela, *Journal of Alloys and Compounds*, 1998, 275–277, 702.

17. ZnO:Zn phosphor for vacuum fluorescent display, HayatoKamikubo (Nec Corporation),*Japan,US 5128063A*, 1992.

18. MarcinNyk , Rajiv Kumar , Tymish Y. Ohulchanskyy , Earl J. Bergey, Paras N. Prasad, *Nano Lett.*, 2008, 8 (11), 3834.

19. M. Avinor, G. Meijer, *Journal of Physics and Chemistry of Solids*, 1960, 12, 211.

20. R. P. Rao, *Journal of Materials Science*, 1986, 21,3357.

21. S. Larach , W. H. McCarroll , R. E. Sharder, *J. Phys. Chem*., 1956, 60 (5), 604.

22. Ting Wang, XuhuiXu, Dacheng Zhou, JianbeiQiu, Xue Yu, *ECS Journal of Solid State Science and Technology*, 2014,3 (8), R139.

23. J. McKittricka, L.E. Sheab, C.F. Bacalskia, E.J. Boszea; *Displays*, 1999, 19,169.

24. Y. Dai, Y. Zhang, Q.K. Li, C.W. Nan, *Chemical Physics Letters*, 2002, 358,83.

25. N.K. Zayer, R. Greef, K. Rogers, A.J.C. Grellier, C.N. Pannell, *Thin Solid Films*, 1999,352,179.

26. Ü. Özgür, Ya. I. Alivov, C. Liu, A. Teke1, M. A. Reshchikov, S. Doğan, V. Avrutin, S.-J. Cho, H. Morkoç, *J. Appl. Phys*.,2005, 98, 041301.

27.HaipingHe, Zhizhen Ye, ShishengLin ,Binghui Zhao and Jingyun Huang*, J. Phys. Chem. C*, 2008, 112 (37), 14262.

28. Dazhi Sun, Minhao Wong, Luyi Sun, Yuntao Li, Nobuo Miyatake, Hung-Jue Sue, *Journal of Sol-Gel Science and Technology,*2007, 43,237.

29. ShrikrushnaShivajiGaikwad, AshishChhaganlal Gandhi, Swarada D. Pandit, Jayashree Pant, Ting-Shan Chan, Chia-Liang Cheng, Yuan-Ron Ma , Sheng Yun Wu, *J. Mater. Chem. C*, 2014, 2, 7264.

30. Yi-Hsuan Lu, Wei-Hao Lin, Chao-Yao Yang, Yi-Hsuan Chiu, Ying-ChihPu, Min-Han Lee, Yuan-Chieh Tseng, Yung-Jung Hsu, *Nanoscale*, 2014,6, 8796.

31. MD McCluskey, SJ Jokela, *J. Appl. Phys*., 2009, 106, 071101.

32. Z. Q. Chen, A. Kawasuso, Y. Xu, H. Naramoto, X. L. Yuan, T. Sekiguchi, R. Suzuki, T. Ohdaira; *Phys. Rev. B*, 2005, 71, 115213.

33. Sajid Ali Ansari, Mohammad Mansoob Khan, ShafeerKalathil, AmbreenNisar, Jintae Lee, Moo Hwan Cho ; *Nanoscale*, 2013,5, 9238.

34. XudongXue, Tao Wang, Xudong Jiang, Jing Jiang, Chunxu Pan, Yichu Wu , *Cryst. Eng. Comm.*, 2014, 16, 1207.

35. D. C. Reynolds, D. C. Look, B. Jogai, C. W. Litton, T. C. Collins, W. Harsch, G. Cantwell, *Phys. Rev. B*, 1998, 57, 12151.

36. ZhigangJia, LinhaiYue, YifanZheng, ZhudeXu, *Materials Chemistry and Physics*, 2008, 107, 137.

37.Noh Soo Han, HyeongSeop Shim, JooHeeSeo, Sun Young Kim, Seung Min Parkand , Jae Kyu Song, *J. Appl. Phys.,* 2010, 107, 084306.

38. P. SundaraVenkatesh, V. Purushothaman, S. EsakkiMuthu, S. Arumugam, V. Ramakrishnan, K. Jeganathan, K. Ramamurthi, *Cryst. Eng. Comm*, 2012, 14, 4713.

39. Zhang Lin-Li, Guo Chang-Xin, Chen Jian-Gang, Hu Jun-Tao, *Chin. Phys*., 2005, 14, 586.

40. X.H. Wang, S.J. Xu, *Applied Physics Letters*, 2013, 102, 181909:1-4.

41. Jianying Shi, Jun Chen, ZhaochiFeng, Tao Chen,Xiuli Wang, Pinliang Ying, and Can Li, *J. Phys. Chem. B*, 2006, 110, 25612.

42. Huang K., *Prog. Phys*. 1981, 1, 31.

43. ShoShirakata ,TokioNakada, *Phys. Status Solidi C 6*, 2009, 5, 1059.

44. Kin Mun Wong, Yaoguo Fang, André Devaux, Liaoyong Wen, Jian Huang, Luisa De Cola and Yong Lei, *Nanoscale*, 3 (2011) 4830.

45. Bingqiang Cao, WeipingCai, GuotaoDuan, Yue Li, Qing Zhao, Dapeng Yu, *Nanotechnology*, 2005,16,2567.

46. Lidia Armelao, Gregorio Bottaro, Michele Pascolini, Michele Sessolo, Eugenio Tondello, Marco Bettinelli, Adolfo Speghini; *J. Phys. Chem. C*, 2008, 112, 4049.

47. G. Ramakrishna, Hirendra N. Ghosh, *Langmuir*, 2003, 19 (7), 3006.

48. SA Studenikin, M Cocivera, *Journal of Applied Physics*, 2002, 91 (8), 5060.

49. Guo-Qing Tang , Ying Xiong, Lei Z. Zhang, Gui-Lan Zhang, *Chemical Physics Letters*, 2004, 395, 97.

50. R. Dingle, *Phys. Rev,* 1969,184,788.

51. D. G. Thomas, J. J. Hopfield, W. M. Augustyniak, *Phys. Rev*., 1965, 140, A202.

52. K. Colbow, *Phys. Rev.,* 1966, 141, 742.

53. M. Soltani, M. Certier., R. Evrard., E. Kartheuser., *J. Appl. Phys*., 1995, 78, 5626.

54. M. Rai, G. Kaur, S. K. Singh, S. B. Rai, *Dalton Trans.*,2015, 44, 6184.

55. The emission spectrum and the radiative lifetime of Eu3+ in luminescent lanthanide complexes, *Phys. Chem. Chem. Phys.*, 2002, 4, 1542.

56. E. Dulkeith, A. C. Morteani, T. Niedereichholz, T. A. Klar, J. Feldmann, S. A. Levi, F. C. J. M. van Veggel, D. N. Reinhoudt, M. Möller, and D. I. Gittins, *Phys. Rev. Lett.,* 2002, 89, 203002.

57. D. Bera, L. Qian, S. Sabui, S. Santra and P.H. Holloway, *Optical Materials*, 2008, 30, 1233.

58. N.S. Norberg and D.R. Gamelin, *J. Phys. Chem B*, 2005, 109, 20810.